Supplementary Information (SI) for Journal of Materials Chemistry A.

Supporting Information

Regenerable and stable conductive topo-polymers for uranium selective extraction

Zilong Wang, Chenzhan Wang,[#] *Xinru Wu, Cichao Yang, Ran Leng, Zhuoyu Ji,*[*]

MOE Key Laboratory of Resources and Environmental System Optimization, College of Environmental Science and Engineering, North China Electric Power University, Beijing, 102206, PR China

[#] These authors contributed equally to this work.

[*] Corresponding authors.

E-mail: jizhuoyu@ncepu.edu.cn (Zhuoyu Ji)

Table of Contents

1. Materials and reagents.

	Chemical Name	**Purity**	**Manufacture**
1	Tetrafluoroterephthalonitrile (TFTPN)	99%	Macklin Biochecal Co., Ltd.
2	Potassium carbonate (K_2CO_3)	99.99%	
3	Hydroxylammonium chloride ($NH_2OH{\cdot}HCl$)	99%	
4	Tetrahydrofuran (THF)	99.5%	
5	N,N-dimethylformamide (DMF)	99.9%	
6	Arsenazo III	95%	
7	Hexa-2,4-diyne-1,6-diol (HDD)	99%	Shanghai Haohong Scientific Co., Ltd.
8	Tetrafluorophthalonitrile (TFPN)	99%	Aladdin Biochemical Technology Co., Ltd
9	Uranyl nitrate hexahydrate ($UO_2\ (NO_3)_2{\cdot}6H_2O$)	99%	
10	4-Nitrophthalonitrile(PN)	99%	
11	Sodium nitrate ($NaNO_3$)	99%	Xi Long Science Co., Ltd.
12	Nickel nitrate ($NiNO_3$)	99%	
13	Calcium nitrate anhydrous ($Ca(NO_3)_2$)	99%	
14	Magnesium nitrate ($Mg(NO_3)_2$)	99%	
15	Strontium nitrate ($Sr(NO_3)_2$)	99%	
16	Barium nitrate ($Ba(NO_3)_2$)	99%	
17	Lanthanum nitrate ($La(NO_3)_3$)	99%	
18	Cerium nitrate ($Ce(NO_3)_3$)	99%	
19	Cobalt dinitrate ($Co((NO_3)_2$)	99%	

20	Cupric nitrate($Cu(NO_3)_3$)	99%	
21	Nafion macromolecule	~5% in a mixture of lower aliphatic alcohols and water	Meryer (Shanghai) Chemical Technology Co., Ltd

Deionized water was prepared from the Millipore system (18.25 MΩ-cm). All the purchased reagents were of analytical grade and used without further purification.

2. Characterization.

Fourier transform infrared spectra (FTIR) of adsorbents were characterized by SHIMADZU-IRT racer-100 spectrometer to determine the functional groups. X-ray photoelectron spectroscopy (XPS) was carried out on Thermo Scientific ESCALAB 250Xi with an Al-alpha excitation source. The surface morphologies of the absorbents were observed with TESCAN MIRA LMS scanning electron microscope (SEM). Thermogravimetric analyses (TGA) were performed on NETZSCH STA 2500 at the temperature range of 25 to 800 °C under nitrogen atmosphere, the heating rate was 10 °C/min. The N_2 adsorption/desorption isotherms were collected at 77 K under a liquid nitrogen bath. The crystal structures were measured in an X-ray diffractometer (Rigaku SmartLab SE) with Cu Kα radiation operated in the 2θ range from 5° to 40°. The zeta potentials of the materials were tested through Malvern Panalytical ZEN 1002. Inductively coupled plasma mass spectrometry (ICP-MS) analyses were carried out on a PerkinElmer NexION 300X spectrometer system. Electrochemical impedance spectroscopy (EIS), Cyclic Voltammetry (CV) and electro-adsorption was carried out by Metrohm Autolab PGSTAT302N with a three-electrode electrochemical cell. The absorption spectra were recorded by Shimadzu, UV-2007 UV-vis absorption spectrometer.

3. Adsorption experiments.

Unless otherwise specified, different aqueous solutions of U(VI) concentrations are obtained by diluting the standard stock $UO_2(NO_3)_2·6H_2O$ solution (300ppm) with a suitable amount of deionized water. The dosage of the adsorption experiments was 0.1 $mg·mL^{-1}$. The pH of the solution was adjusted by HNO_3 or $NaNO_3$ aqueous solution. Except for the influence of pH experiments, all the adsorption experiments were conducted under the pH=5. Subsequently, the centrifuge tube was oscillated at a constant temperature of 25°C and a speed of 150 r.p.m. in a shaking incubator for 3 hours. After adsorption, the mixtures were filtered by a syringe filter (0.22 μm membrane filter). The concentrations of U(VI) in the filtrates were analyzed by Arsenazo III based colorimetric analysis method. The adsorption capacity (q_e, $mg·g^{-1}$), removal rate (r, %) and distribution coefficient value (K_D, mL g^{-1}) were calculated according to the following Eqs:

$$q_e = \frac{(c_0 - c_e) \times v}{m} \quad (1)$$

$$r = \frac{c_0 - c_e}{c_0} \times 100\% \quad (2)$$

where c_0 ($mg·L^{-1}$) is the initial concentrations; c_e is the equilibrium concentrations ($mg·L^{-1}$); v (L) is the volume of the adsorption solution; m (g) is the weight of the adsorbent.

3.1 Uranium adsorption isotherms

3.1.1 Uranium adsorption isotherms in deionized water.

To obtain the adsorption isotherms of uranium, the experiments were performed under the required initial U(VI) concentrations (20 to 140 mg L^{-1}) at 25°C. Langmuir and Freundlich equations were applied to fit the equilibrium isotherms.

Langmuir isotherm:

$$q_e = \frac{K_L q_{max} c_e}{1 + K_L c_e} \tag{3}$$

Freundlich isotherm:

$$q_e = K_f c_e^{\frac{1}{n}} \tag{4}$$

where q_e is the uptake ($mg \cdot g^{-1}$) of uranium and c_e is the concentrations ($mg \cdot L^{-1}$) of U(VI) at equilibrium; q_{max} is the saturation adsorption capacity ($mg \cdot g^{-1}$) which represents the maximum U(VI) adsorption amount of the adsorbents. K_L ($L \cdot g^{-1}$) is the equilibrium constant in Langmuir equation. K_f (L $mg \cdot g^{-1}$ $mg^{-1/n}$) and $1/n$ are both constants in Freundlich equation which are related to adsorption capacity and intensity.

3.1.2 Uranium adsorption isotherms in U- spiked seawater.

To obtain the adsorption isotherms of uranium in U- spiked seawater, the deionized water was replaced with filtered seawater in the experiments and other conditions were consistent with the deionized water experiment.

3.2 Uranium adsorption kinetics

To obtain the uranium adsorption kinetic, U(VI) aqueous solution (19.2 mL, 300 $mg \cdot L^{-1}$) and $NaNO_3$ aqueous solution (1.6 mL, 3 $mol \cdot L^{-1}$) were added to a thermostatic oscillating tank, the pH of the solution was pre-adjusted to 5. Meanwhile, 4.8 mg adsorbent was dispersed in deionized water (27.2 mL, 0.1 $mg \cdot L^{-1}$, pH=5). Then add the adsorbent solution to the uranyl solution and start the timer. The U(VI) concentrations of different times (0.5, 1, 3, 5, 15, 30, 60, 90, 120, 180, 240, 300 min) were determined immediately. Pseudo-first order and pseudo-second order rate models were applied to fit the kinetics data. The equations are given as follows:

Pseudo-first order equation:

$$\ln{(q_e - q_t)} = \ln{q_e} - k_1 t \tag{5}$$

Pseudo-second order equation:

$$\frac{t}{q_t} = \frac{t}{q_e} + \frac{1}{k_2 q_e^2} \tag{6}$$

where q_e is the equilibrium adsorption capacity (mg·g^{-1}). q_t represents the uptake (mg·g^{-1}) of U(VI) at required time (t). k_1 and k_2 are the rate constants of pseudo-first order and pseudo-second order model.

3.3 The influence of the pH experiment

The influence of pH experiment was performed in 120 ppm uranium aqueous solution with different pH (2.0, 3.0, 4.0, 5.0, 6.0, 7.0, 8.0, 9.0). After 3 hours, the solution was filtered and the concentrations of U(VI) in the filtrates were analyzed by Arsenazo III based colorimetric analysis method.

3.4 Stability experiments.

To test the stability, the adsorbent was dispersed in seawater, alkaline solutions (1 M and 3 M NaOH aqueous solution) and acidic solutions (1 M and 3 M HNO_3 and HCl aqueous solution) for 12 hours, respectively. The mixture was filtered and thoroughly wash with deionized water. Then the adsorbent was dried through vacuum freeze drying and measured by

FT-IR spectroscopy. The adsorption capacity was analyzed by Arsenazo III based colorimetric analysis method mentioned in ***3.1***.

3.5 Recyclability experiments.

Carbonate solution system is one of the common methods for extraction of uranyl ions,[1, 2] primarily due to its ability to effectively desorb uranium from adsorbent materials and its relatively mild and environmentally friendly nature. [3, 4]

The specific mechanisms and advantages include: 1) *Formation of Soluble Complexes.* Sodium carbonate provides carbonate ions (CO_3^{2-}), which can form soluble complexes with UO_2^{2+}, such as $UO_2(CO_3)_3$. This complexation helps to release uranium from the adsorbent material, facilitating its recovery. 2) *pH Regulation.* The alkaline nature of sodium carbonate solution helps to maintain a high pH, which is often necessary for the desorption process. Higher pH levels can disrupt the binding interactions between UO^2 and the adsorbent, making it easier to elute the uranium. 3)*Environmental and Economic Advantages.* Sodium carbonate is less corrosive compared to other strong bases like sodium hydroxide (NaOH). It is also more environmentally friendly and cost-effective, making it a preferred choice for industrial-scale regeneration processes. 4) *Enhanced Adsorbent Reusability.* The regeneration process using sodium carbonate solution is relatively gentle on the adsorbent material, preserving its structural integrity and functional groups. This allows for multiple cycles of adsorption and desorption, improving the overall efficiency and economic viability of the process.

To test the recyclability of the adsorbent, 39.0 mg adsorbent was dispersed in 364 mL deionized water in a bottle, then U(VI) aqueous solution (13 mL, 300 mg·L^{-1}) and $NaNO_3$ aqueous solution (13 mL, 3 mol·L^{-1}) were added to the bottle. The final volume was 390 mL and the dosage of adsorbent was 0.1 mg·mL^{-1}. The pH of the solution was adjusted to 5. The bottle was then shaken at a constant temperature of 25°C and 150 r.p.m. for 3 hours in a thermostatic shaking incubator. After vacuum filtration, the loaded sample was dispersed in 200 mL of Na_2CO_3 (0.5 mol·L^{-1}) aqueous solution for 12h to desorb the U(VI). Subsequently, the adsorbent was filtered under reduced pressure and freeze-dried for next adsorption of U(VI) to test the recyclability until eighth cycle.

3.6 The influence of ion competition

3.6.1 The influence of ion competition in spiked natural seawater

The selectivity test of U(VI) adsorption from spiked seawater containing VO^{3-}, Cu^{2+}, Mg^{2+}, Ni^{2+}, Sr^{2+}, Ba^{2+}, Co^{2+}, La^{3+}, Ce^{3+} and U(VI) was carried out at pH=5.0. The initial concentration of each metal ion is 100 ppm, and the residual metal ions concentration in the filtrates was determined by inductively coupled plasma-mass spectrometry (ICP-MS).

The partition coefficient K_D is a valuable parameter for determining the affinity and selectivity performance, which is calculated by Eq. (7):

$$K_D = \frac{(c_0 - c_e)}{c_e} \times \frac{v}{m} \tag{7}$$

where c_0 (mg·L^{-1}) is the initial concentrations; c_e (mg·L^{-1}) *is the* equilibrium concentrations; *v* (mL) is the volume of the adsorption solution; m (mg) is the weight of the adsorbent.

3.6.2 The influence of ion competition in simulated natural seawater.

The selectivity test of U(VI) adsorption from 100× spiked natural seawater containing UO_2^{2+}, VO^{3+}, Co^{2+}, Ni^{2+}, Cu^{2+} and Sr^{2+} was carried out at pH=5.0. The 100× spiked natural seawater was prepared by adding co-existing metal ions in the filtered natural seawater. The concentration of each competing ions is 100 times than its real concentration in the natural sea water, and the residual metal ions concentration in the filtrates was determined by inductively coupled plasma-mass spectrometry (ICP-MS). The partition coefficient is calculated by Eq. (7).

3.7 Extraction of uranium from natural seawater.

1 mg HDD-TFPTN-AO was sealed in a dialysis bag and immersed in 2 L of filtered natural seawater from East China Sea, the seawater is replaced every five days. After 25 days of enrichment, the adsorbent loaded with uranium was dissolved in 10 mL of aqua regia. Then, 1mL of the solution was diluted to 5 mL by 0.3 M HNO_3. The concentration of uranium in the diluted solution was determined by inductively coupled plasma-mass spectrometry (ICP-MS).

3.8 Electrochemical performance test and alternating current electrochemical (AACE) method for uranium adsorption.

The electrochemical performance of HDD-TFTPN-AO was measured in a three-electrode cell with the supporting electrolyte forming of 1 M Na_2SO_4 and 10 mM $K_4Fe(CN)_6$ aqueous solution. 1×1cm^2 hydrophilic conductive carbon cloth containing 1mg adsorbent was used as the working electrode, the graphite electrode was used as the counter electrode and the saturated calomel electrode was used as the reference electrode.

The device in adsorption experiments were similar to the electrochemical performance test, the working electrode was changed to 2×2 cm^2 hydrophilic conductive carbon cloth containing 0.5mg adsorbent and the supporting electrolyte was replaced with 0.01 M $NaNO_3$ containing 60 ppm U aqueous solution. Under the alternating current electrochemical (AACE) method, the voltage alternates were between -1.3 V and 0 V, and the duration times were 0.5 ms and 2 ms, respectively. The AACE method avoids the evolution of hydrogen gas (HER reaction), to prevent the affect the enrichment of uranyl ions.[5] Both the AACE method and the physicochemical adsorption were under the condition of pH=5 and 25°C.

4. Figures

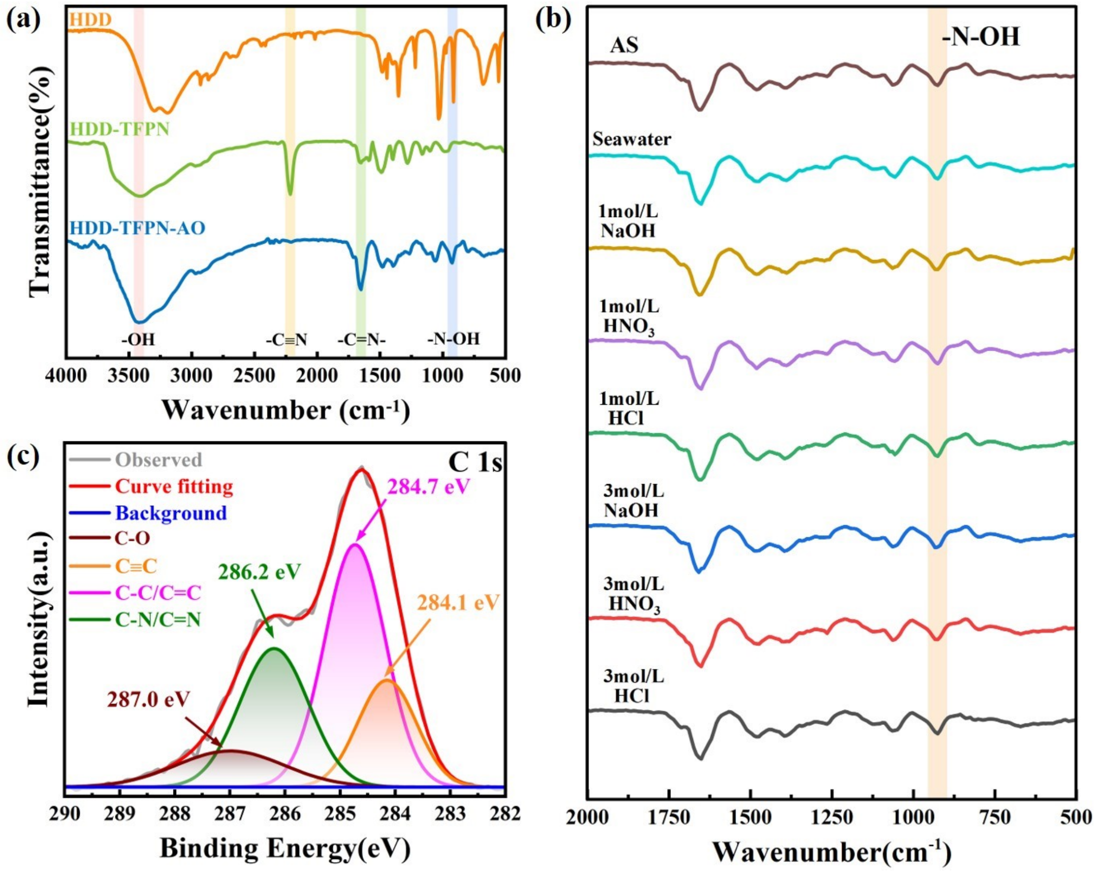

Figure S1. Characterization of **HDD-TFPN-AO**. (a) FT-IR spectra of HDD, **HDD-TFPN** and **HDD-TFPN-AO**. (b) FT-IR spectra of **HDD-TFPN-AO** after treatment by different conditions. (c) XPS spectra of C1s for **HDD-TFPN-AO**.

The appearance of the characteristic peaks of C≡N and C-O at 2220 cm^{-1} and 1249 cm^{-1} indicates the effective polymerization of HDD-TFPN. The disappearance of the characteristic peaks of C≡N combined with the result of XPS further proves the successful amidoximation by $NH_2OH \cdot HCl$. Unchanged peaks in FTIR after treatment with harsh conditions demonstrate the good chemostability of the adsorbents.

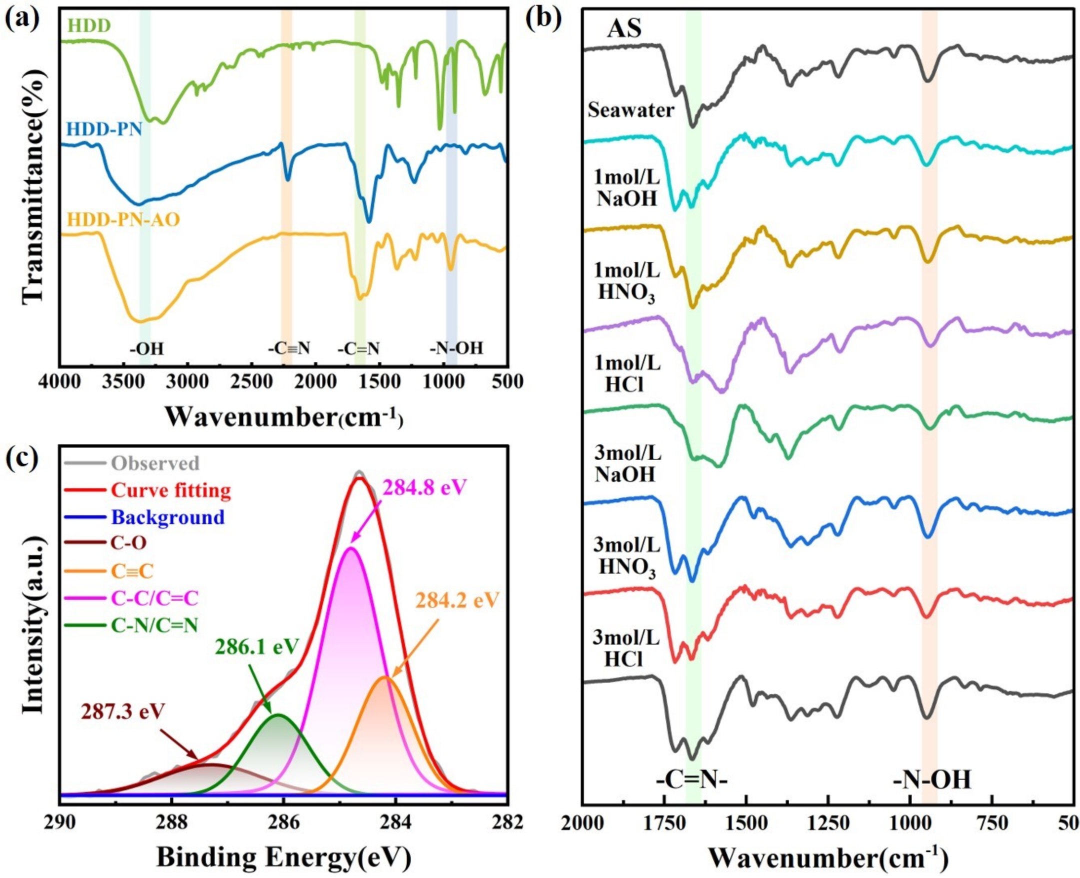

Figure S2. Characterization of **HDD-PN-AO**. (a) FT-IR spectra of HDD, **HDD-PN** and **HDD-PN-AO**. (b) FT-IR spectra of **HDD-PN-AO** after treatment by different conditions. (c) XPS spectra of C1s for **HDD-PN-AO**.

The appearance of the characteristic peaks of $C\equiv N$ and C-O at 2220 cm^{-1} and 1249 cm^{-1} indicates the effective polymerization of HDD-PN. The disappearance of the characteristic peaks of $C\equiv N$ combined with the result of XPS further proves the successful amidoximation by $NH_2OH\cdot HCl$. Unchanged peaks in FTIR after treatment with harsh conditions demonstrate the good chemostability of the adsorbents.

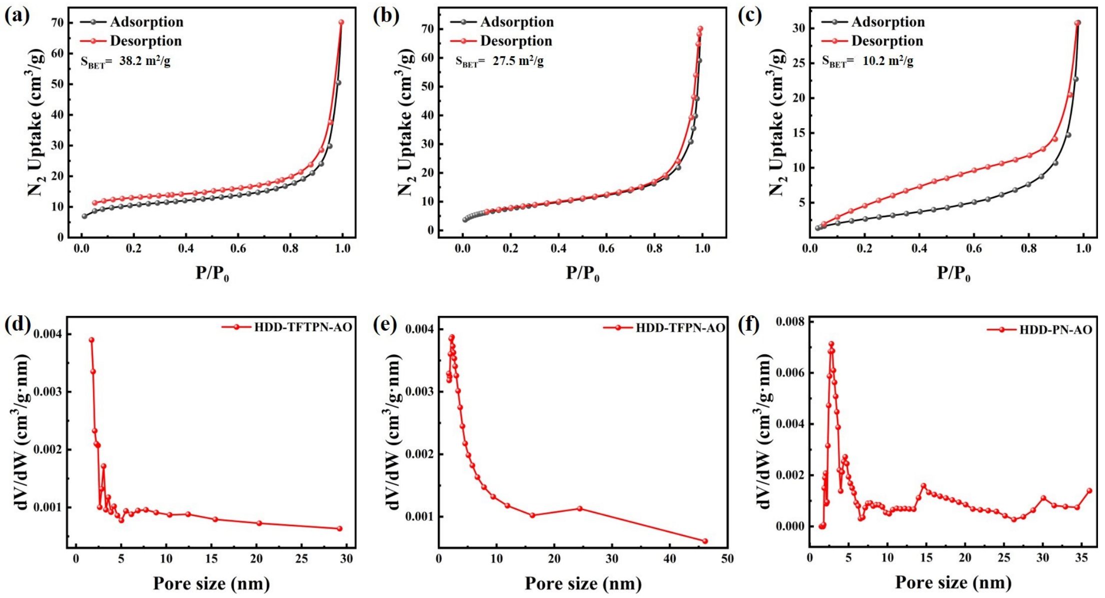

Figure S3. N_2 adsorption-desorption isotherms of **HDD-TFTPN-AO** (a), **HDD-TFPN-AO** (b) and **HDD-PN-AO** (c). Pore size distribution of **HDD-TFTPN-AO** (d), **HDD-TFPN-AO** (e) and **HDD-PN-AO** (f).

BET data were collected at 77 K under a liquid nitrogen bath. The pore size of three TP-COPs match with the calculated results.

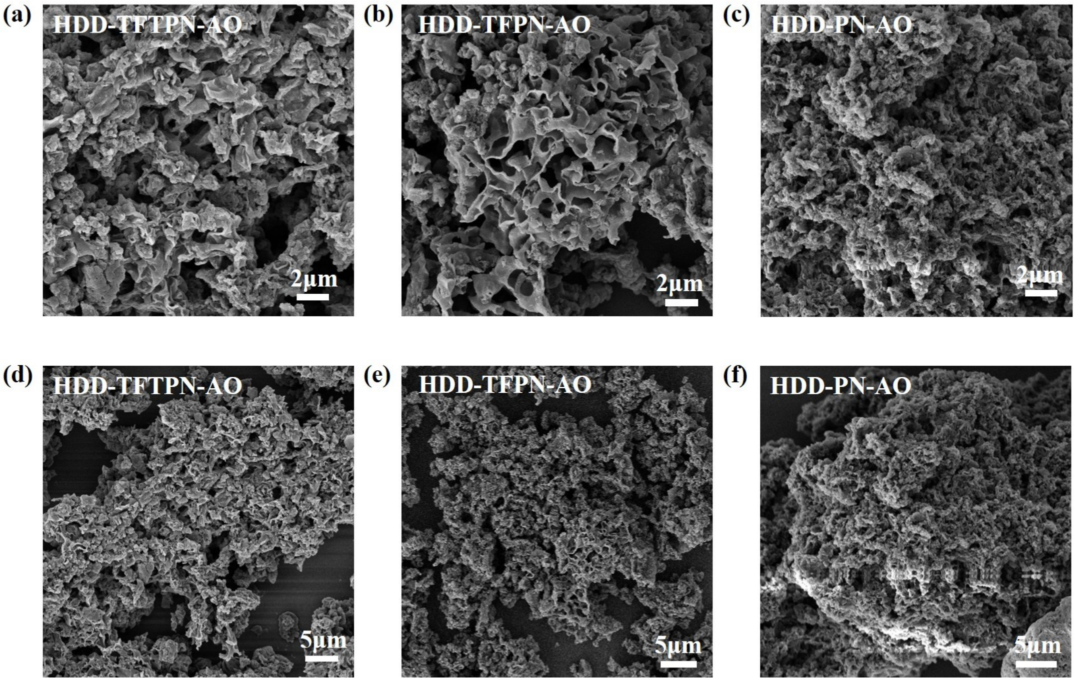

Figure S4. SEM images of **HDD-TFTPN-AO** (a), (d), **HDD-TFPN-AO** (b), (e) and **HDD-PN-AO** (c) (f).

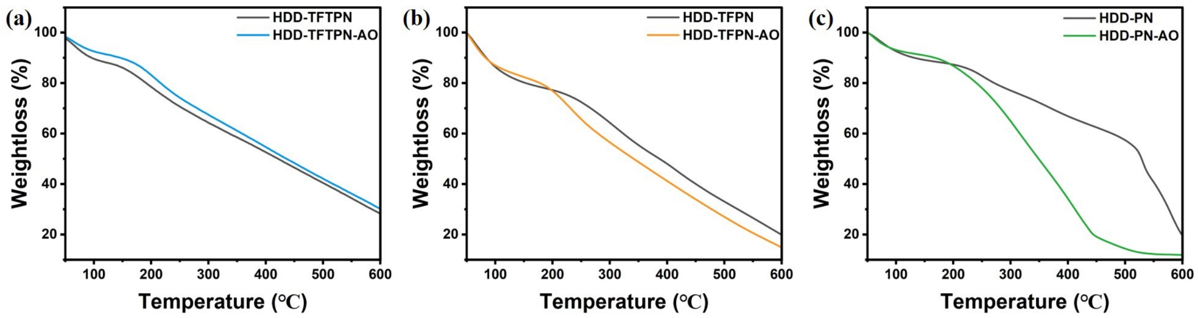

Figure S5. TGA curves of **a). HDD-TFTPN** and **HDD-TFTPN-AO b). HDD-TFPN** and **HDD-TFPN-AO c). HDD-PN** and **HDD-PN-AO**

TGA was measured under nitrogen atmosphere with heating rate as 10 °C·min^{-1}. The mass loss of the first stage can be ascribed to the physically adsorbed water or solvents. The mass drop between 100 °C and 200 °C is due to the degradation of the amidoxime groups and TFTPN. The last stage results from the decomposition of the skeleton of the adsorbents.

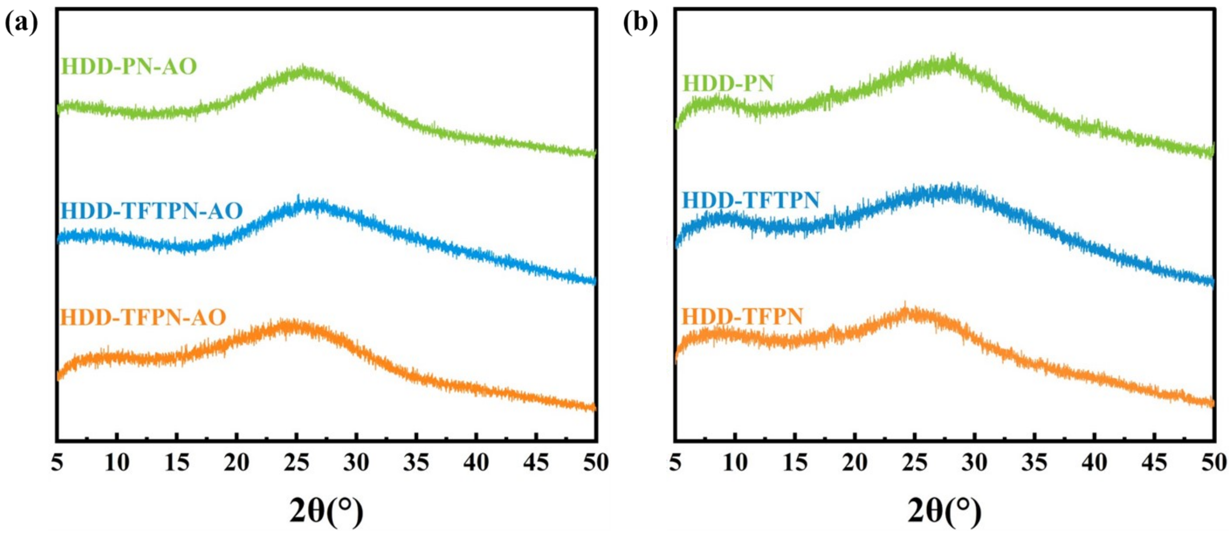

Figure S6. a) XRD patterns of **HDD-TFTPN-AO**, **HDD-TFPN-AO** and **HDD-PN-AO**. **b)** XRD patterns of **HDD-TFTPN**, **HDD-TFPN** and **HDD-PN**.

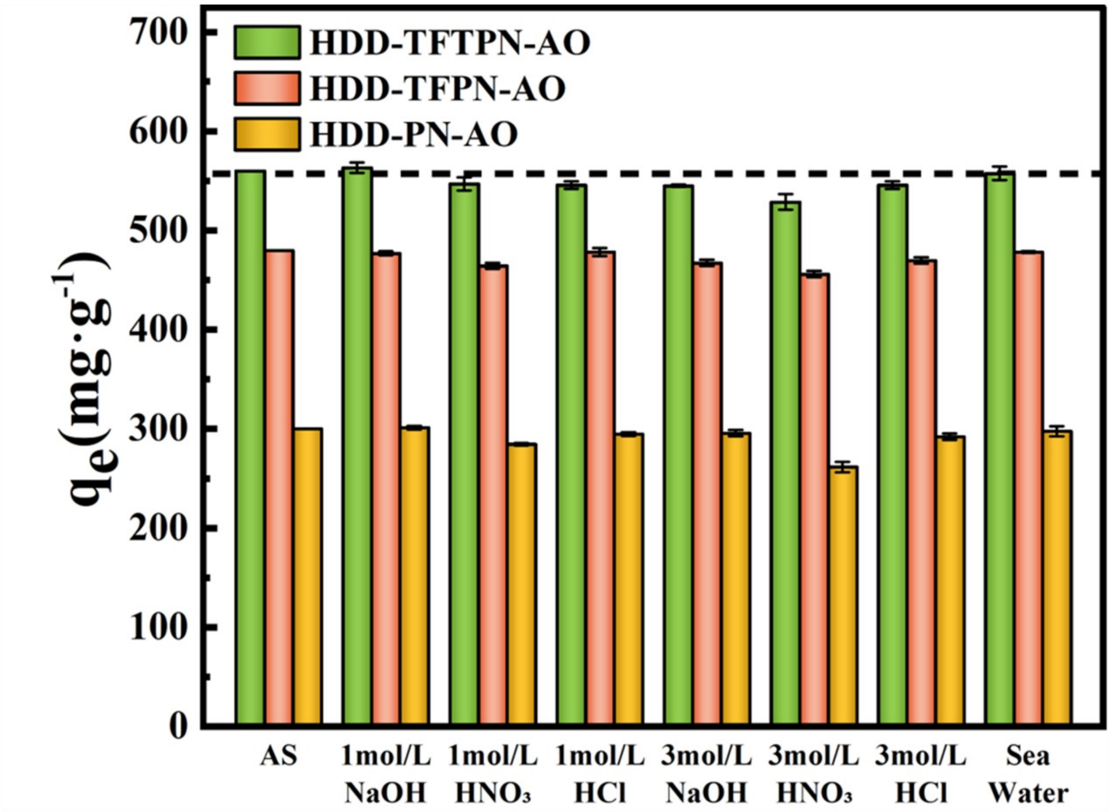

Figure S7. The adsorption capacity of the COPs after treatment under different harsh conditions.

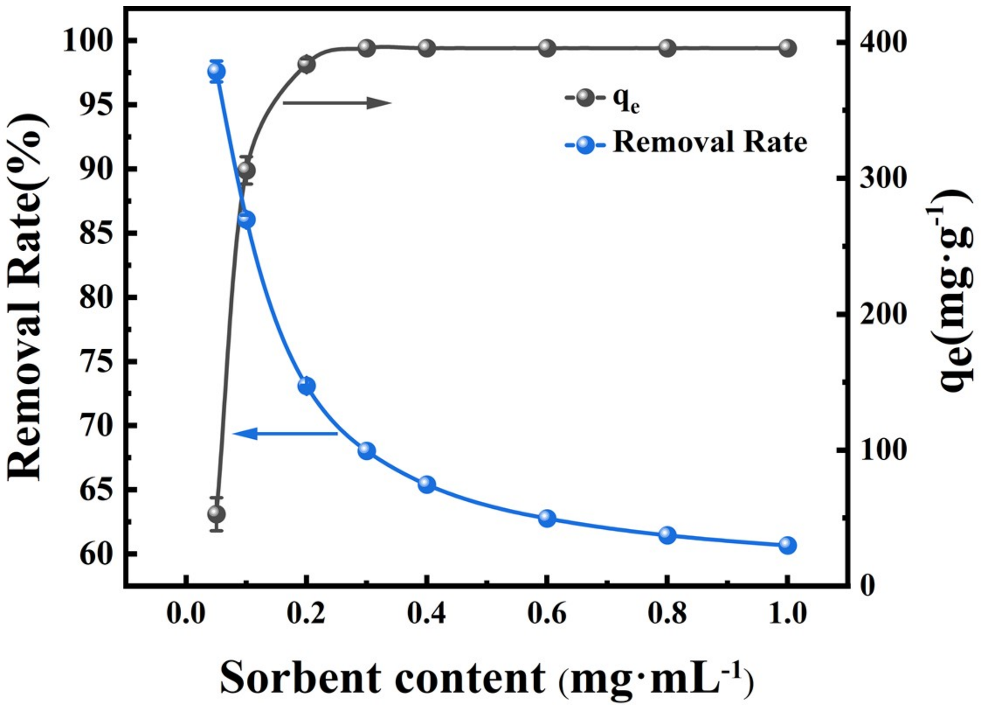

Figure S8. The removal rate and the adsorption capacity of **HDD-TFTPN-AO** under different adsorbent content. (0.01 mol·L^{-1} $NaNO_3$, 20 ppm U(VI), pH=5, 25 °C, 3 h).

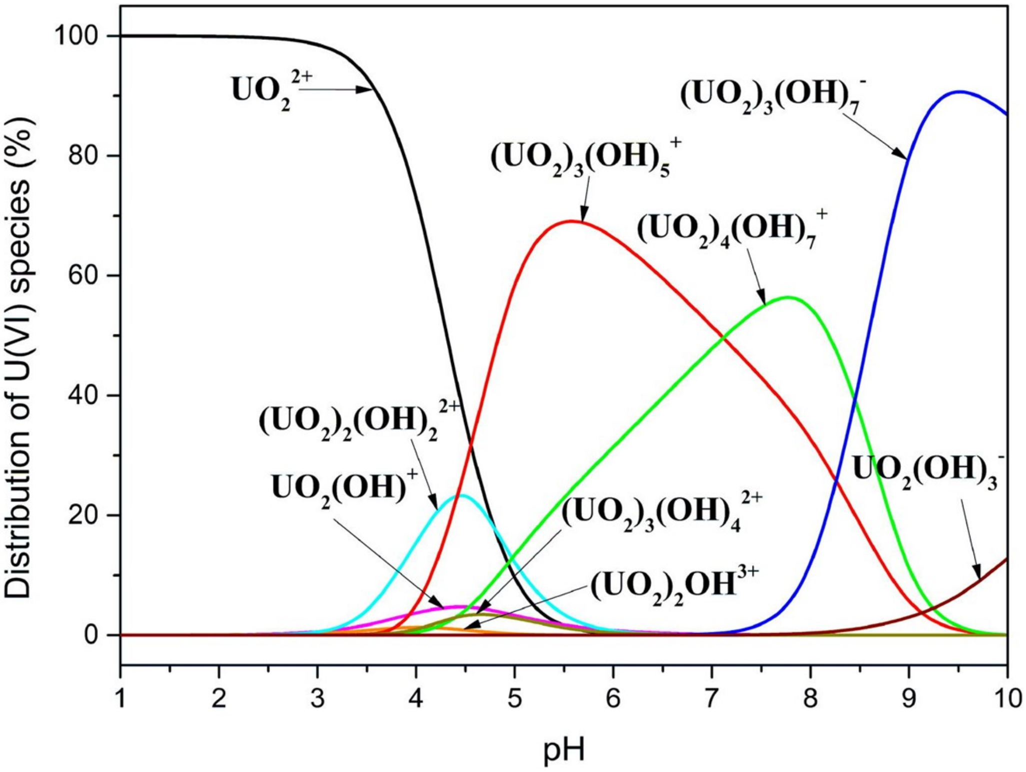

Figure S9. The distribution of aqueous U(VI) species as a function of $pH_{initial}$, C_0 = 150 mg·L^{-1}, T = 303.15 K.[6]

The aqueous solution of uranium can hydrolyze at a higher pH value. At pH<3.7, UO_2^{2+} is the main U (VI) substance in aqueous solution. When the pH ranges from 3.7 to 7.5, the proportion of polynuclear uranyl hydrate ions increased due to the coordination between hydroxyl group and UO_2^{2+} ions and the partial polymerized hydrolysis products indeed exist in form of colloid. At pH=6, $(UO_2)_3(OH)_5^+$ and $(UO_2)_4(OH)_7^+$ carrying larger U(VI) ionic radii than hydrated uranyl ion (~6.4 Å) present as the main speciation of U(VI). And small proportion of $(UO_2)_2(OH)_2^{2+}$, UO_2OH^+ and UO_2CO_3 (aq) exist simultaneously in the system.

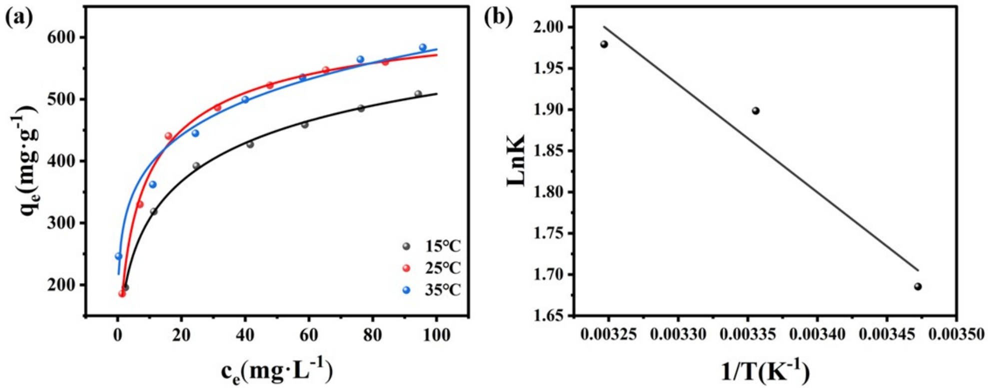

Figure S10. (a) Thermodynamic curve of adsorption of uranyl ion by HDD-TFTPN-AO (pH=5). **(b)** Thermodynamic fitting of adsorption of uranyl ion by HDD-TFTPN-AO.

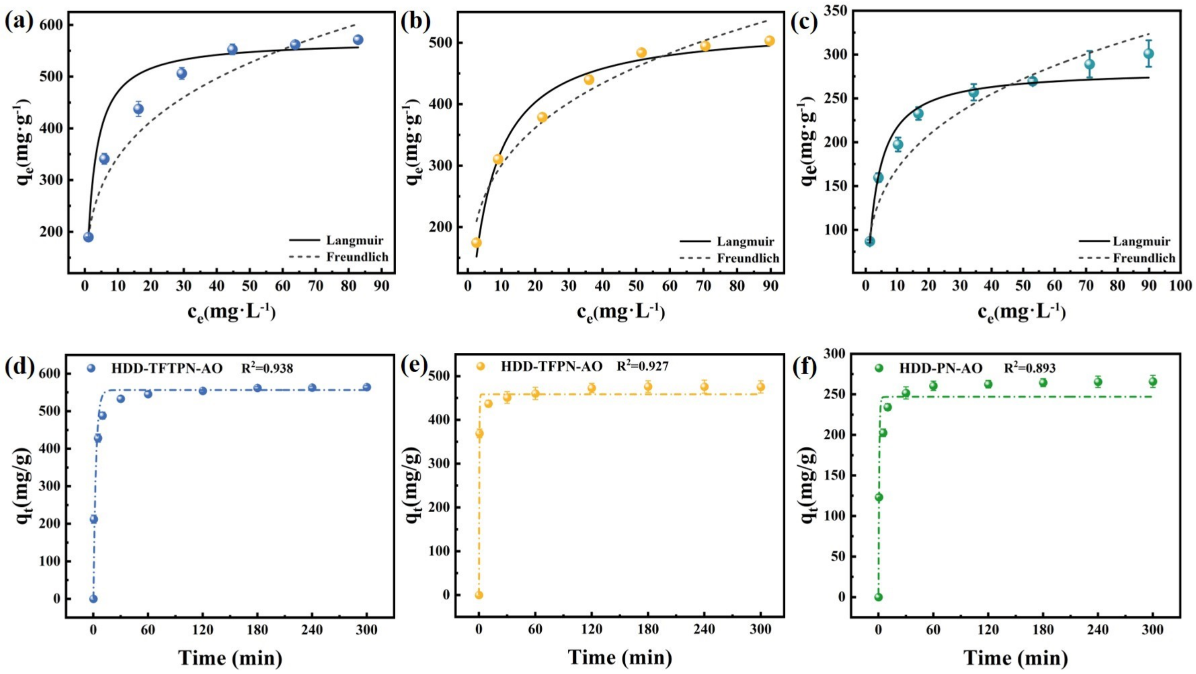

Figure S11. Adsorption isotherm of **HDD-TFTPN-AO** (a), **HDD-TFPN-AO** (b) and **HDD-PN-AO** (c) with Langmuir and Freundlich isotherm model fitting for experimental data. Pseudo-first-order kinetic model fit for uranium adsorption of **HDD-TFTPN-AO** (d), **HDD-TFPN-AO** (e) and **HDD-PN-AO** (f). Error bars represent S.D. n=3 independent experiments.

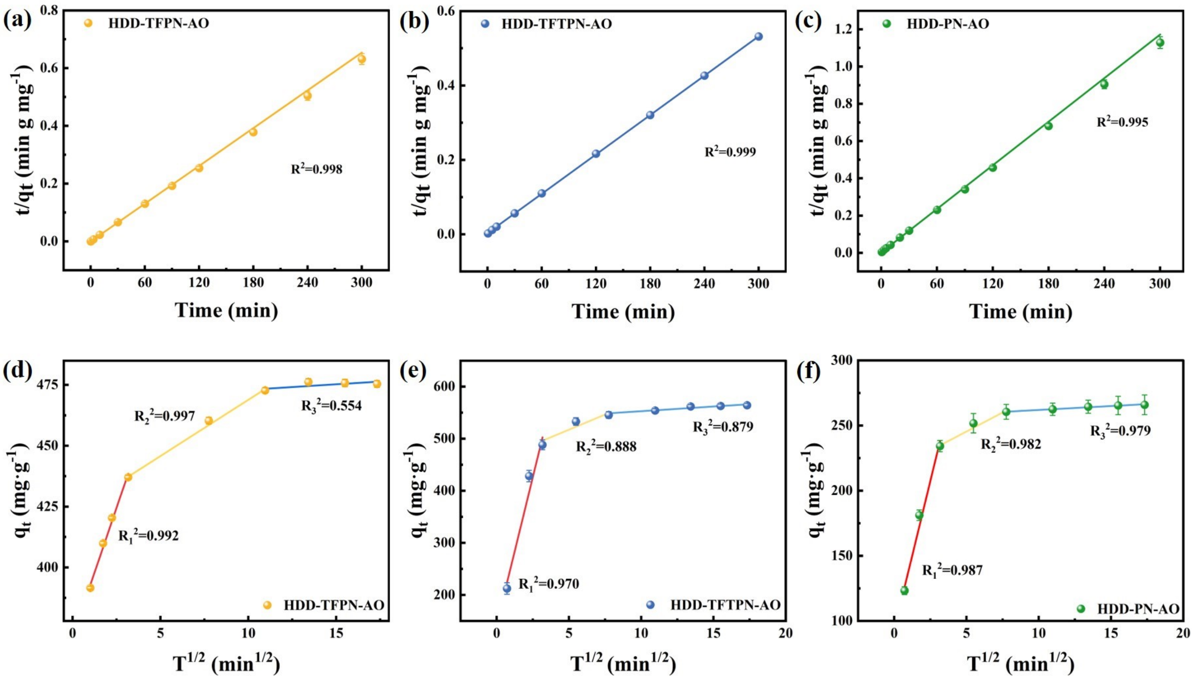

Figure S12. Pseudo-second-order kinetic model fit for uranium adsorption of **HDD-TFTPN-AO** (a), **HDD-TFPN-AO** (b) and **HDD-PN-AO** (c). Intraparticle diffusion model fit for uranium adsorption of **HDD-TFTPN-AO** (d), **HDD-TFPN-AO** (e) and **HDD-PN-AO** (f). Error bars represent S.D. n=3 independent experiments.

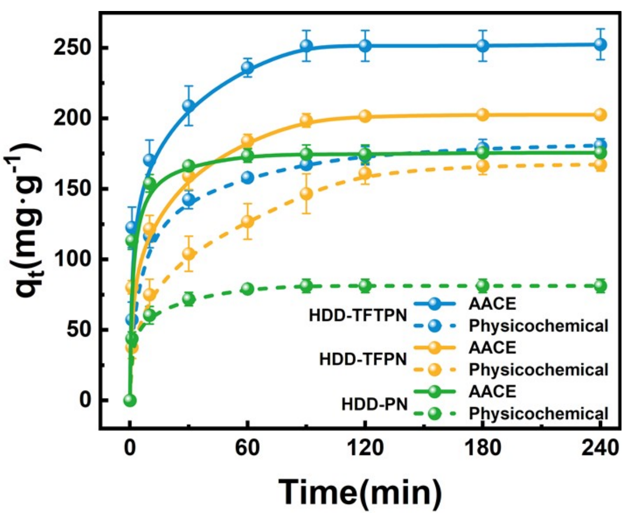

Figure S13. Uranium adsorption of three TP-COPs before amidoximation using the AACE and the physical diffusion methods

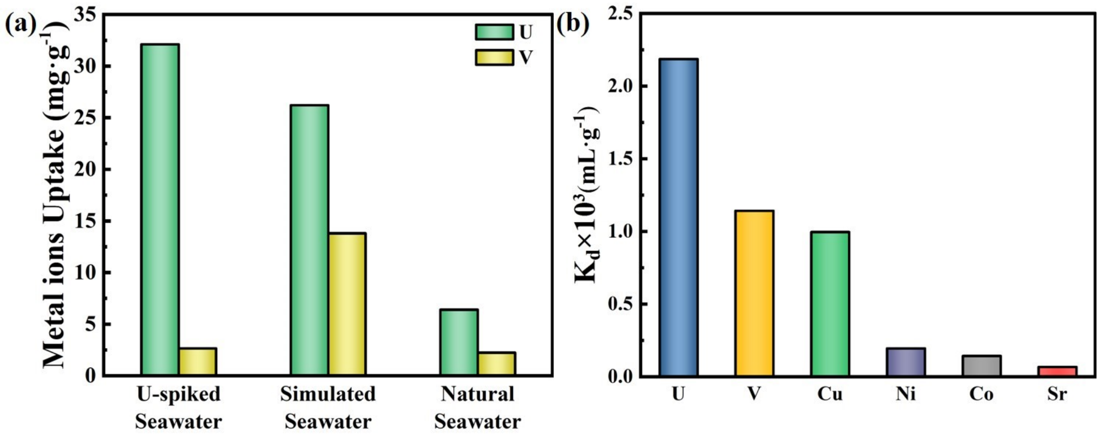

Figure S14. (a) Uranium extraction capacity of **HDD-TFTPN-AO** in 100×U-spiked seawater, simulated seawater and natural seawater. (b) Selectivity of **HDD-TFTPN-AO** in simulated seawater.

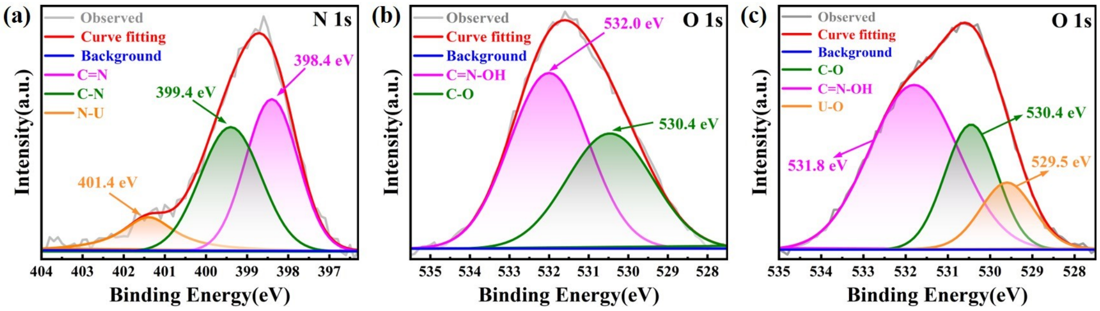

Figure S15. (a) XPS spectra of N1s for **HDD-TFTPN-AO** with U-loaded. (b) XPS spectra of O1s for **HDD-TFTPN-AO**. (c) XPS spectra of O1s for **HDD-TFTPN-AO** with U-loaded.

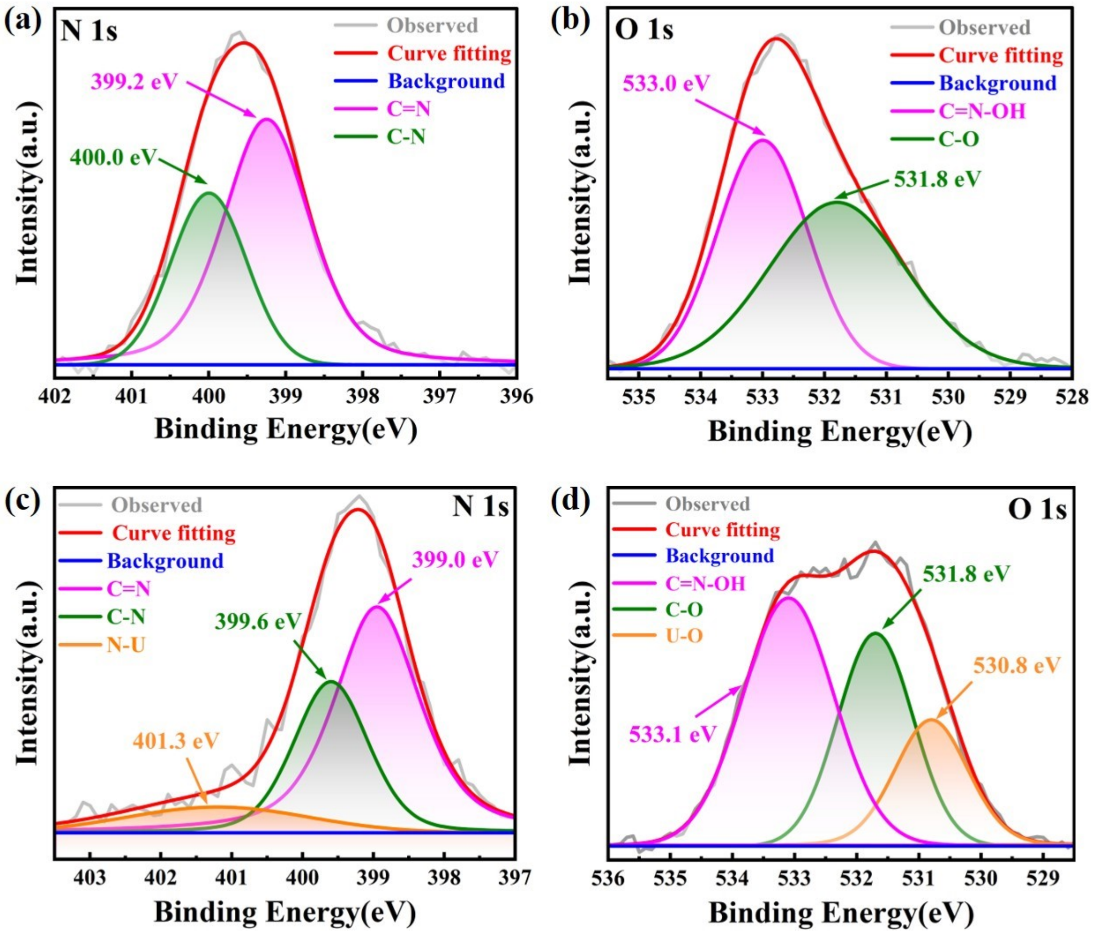

Figure S16. (a) XPS spectra of N1s for **HDD-TFPN-AO**. (b) XPS spectra of O1s for **HDD-TFPN-AO**. (c) XPS spectra of N1s for **HDD-TFPN-AO** with U-loaded. (d) XPS spectra of O1s for **HDD-TFPN-AO** with U-loaded.

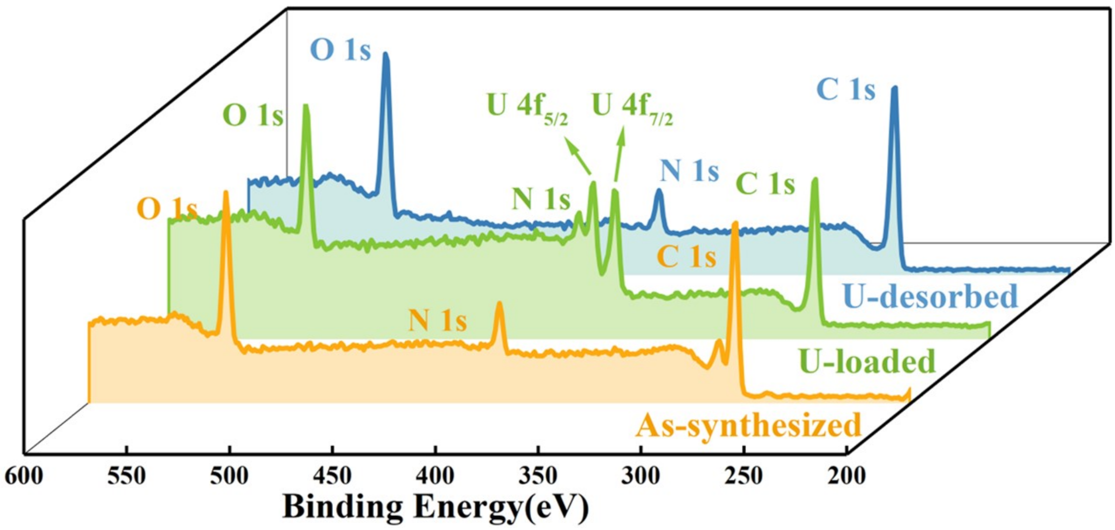

Figure S17. XPS survey spectra of **HDD-TFPN-AO** after uranium adsorption and desorption.

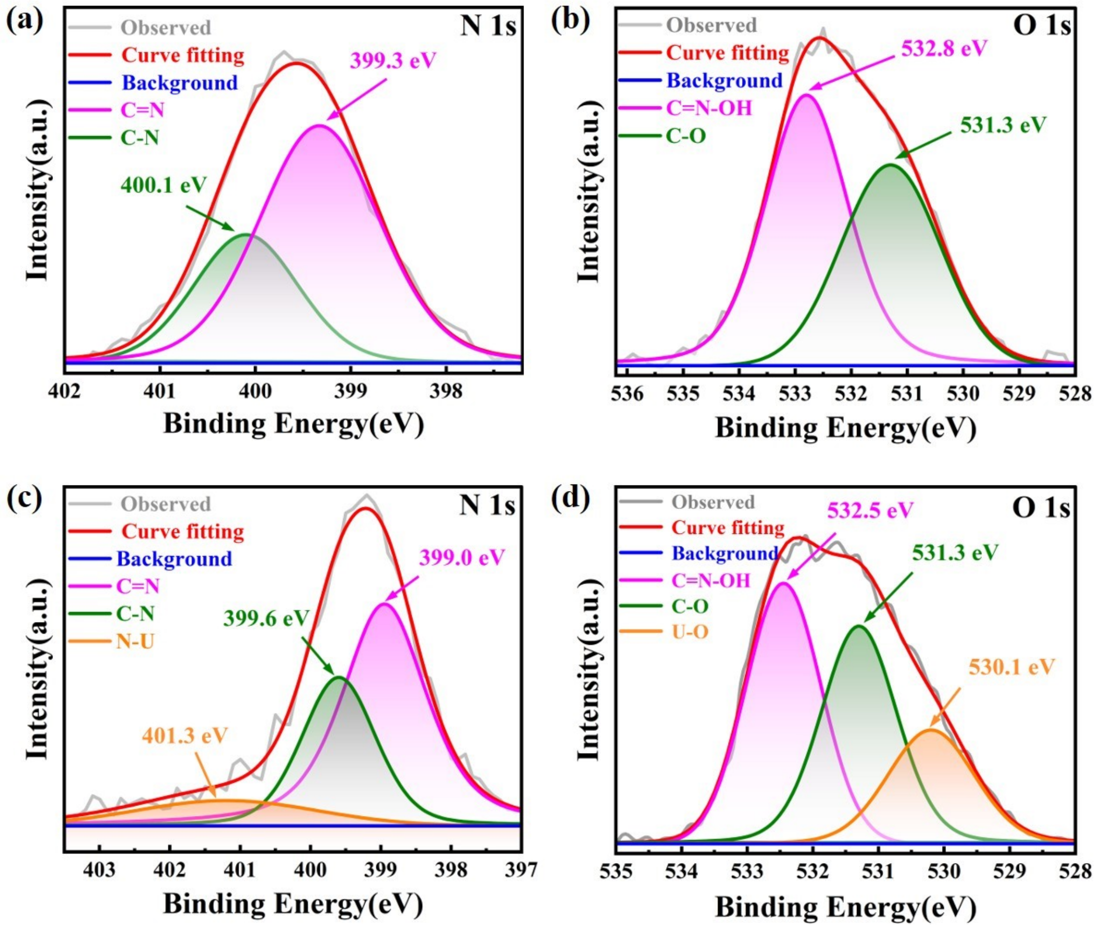

Figure S18. (a) XPS spectra of N1s for **HDD-PN-AO**. (b) XPS spectra of O1s for **HDD-PN-AO**. (c) XPS spectra of N1s for **HDD-PN-AO** with U-loaded. (d) XPS spectra of O1s for **HDD-PN-AO** with U-loaded.

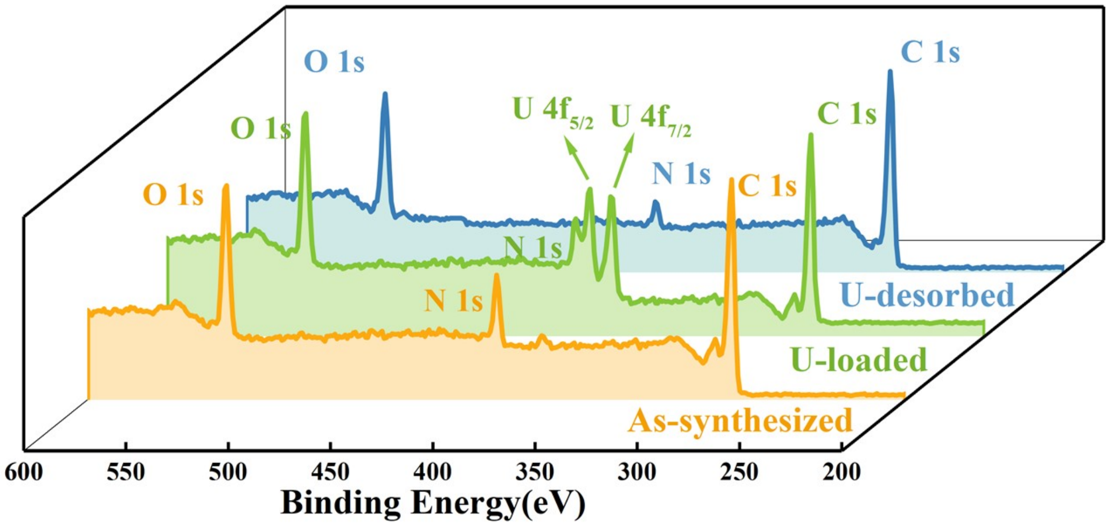

Figure S19. XPS survey spectra of **HDD-PN-AO** after uranium adsorption and desorption.

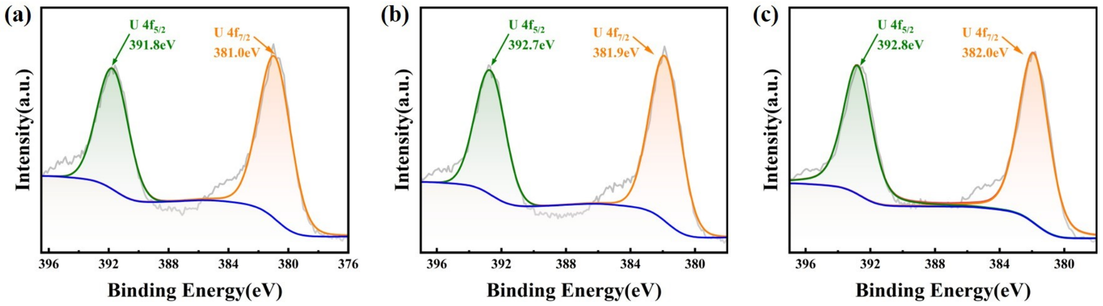

Figure S20. U 4f high-resolution spectra of **HDD-TFTPN-AO** (a), **HDD-TFPN-AO** (b) and **HDD-PN-AO** (c) with U-loaded.

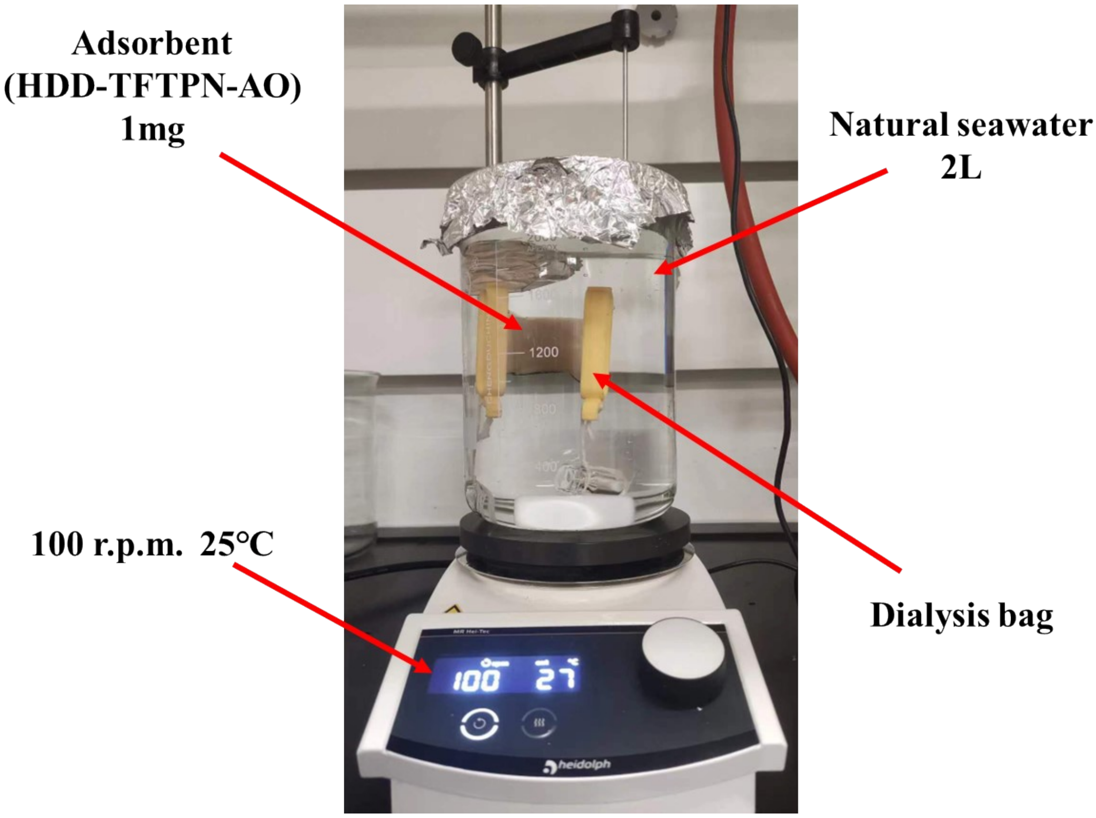

Figure S21. Device for uranium extraction in natural seawater.

1 mg HDD-TFPTN-AO was sealed in a dialysis bag and immersed in 2 L of filtered natural seawater from East China Sea, the seawater is replaced every five days. After 25 days of enrichment, the adsorbent loaded with uranium was dissolved in 10 mL of aqua regia. Then, 1mL of the solution was diluted to 5 mL by 0.3 M HNO3. The concentration of uranium in the diluted solution was determined by inductively coupled plasma-mass spectrometry (ICP-MS).

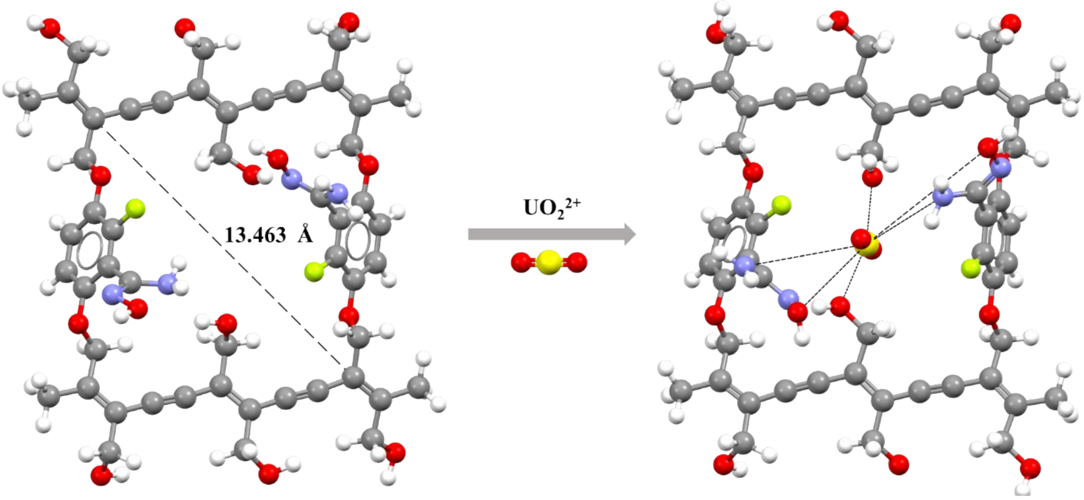

Figure S22. DFT calculation of **HDD-TFTPN-AO**

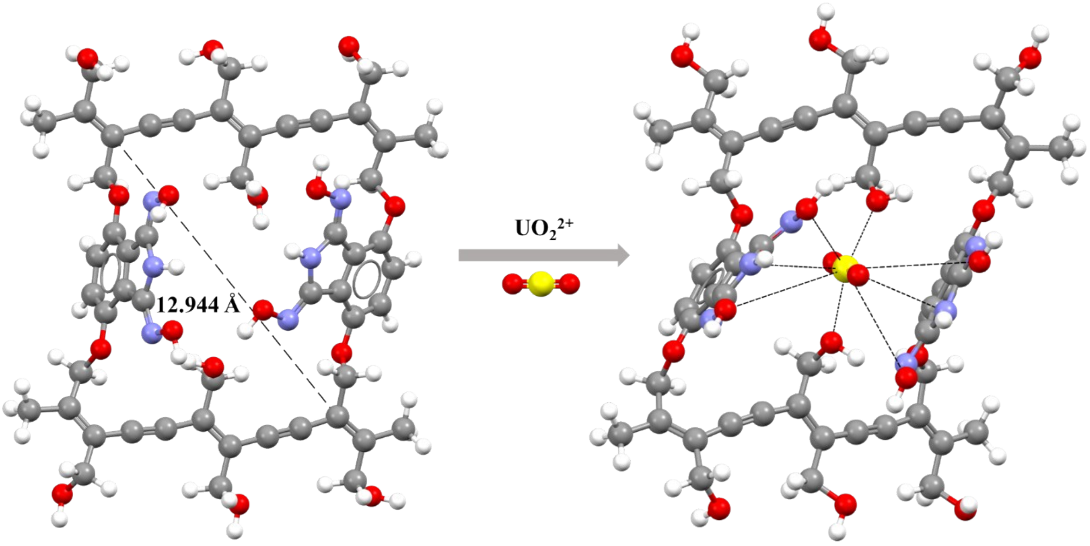

Figure S23. DFT calculation of **HDD-TFPN-AO**

All the density-functional theory (DFT) computations were performed using the Dmol3 software package based on the linear combination of atomic orbitals (LCAO) method. Electron-ion interactions were described using the DSPP potentials. A double numerical polarized (DNP) basis set was employed to expand the wave functions with an orbital cutoff of 5.9 Å. For the electron-electron exchange and correlation interactions, the BP functional was used throughout.

During the geometry optimizations, all the atoms were allowed to relax. In this work, the convergence criterion for the electronic self-consistent field (SCF) loop was set to 10^{-6}. The atomic structures were optimized until the residual forces were below 0.002 Ha Å^{-1}.

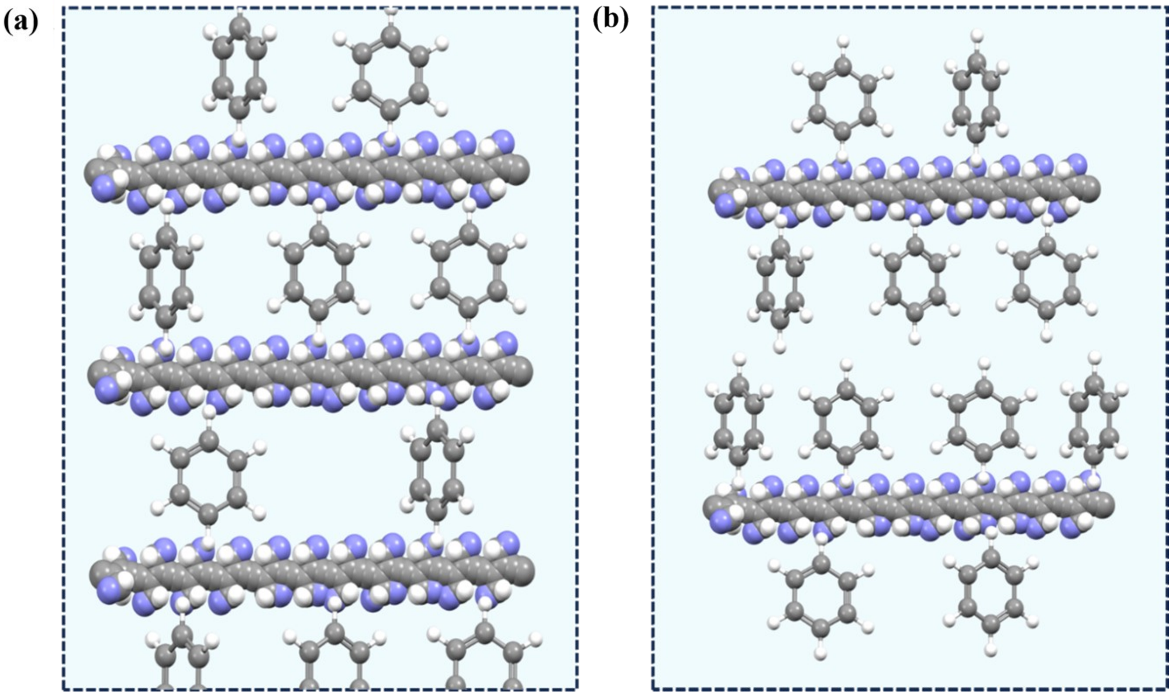

Figure S24. Schematic illustration of the difference in structure between **HDD-TFTPN-AO** or **HDD-TFPN-AO (a)** with **HDD-PN-AO (b).**

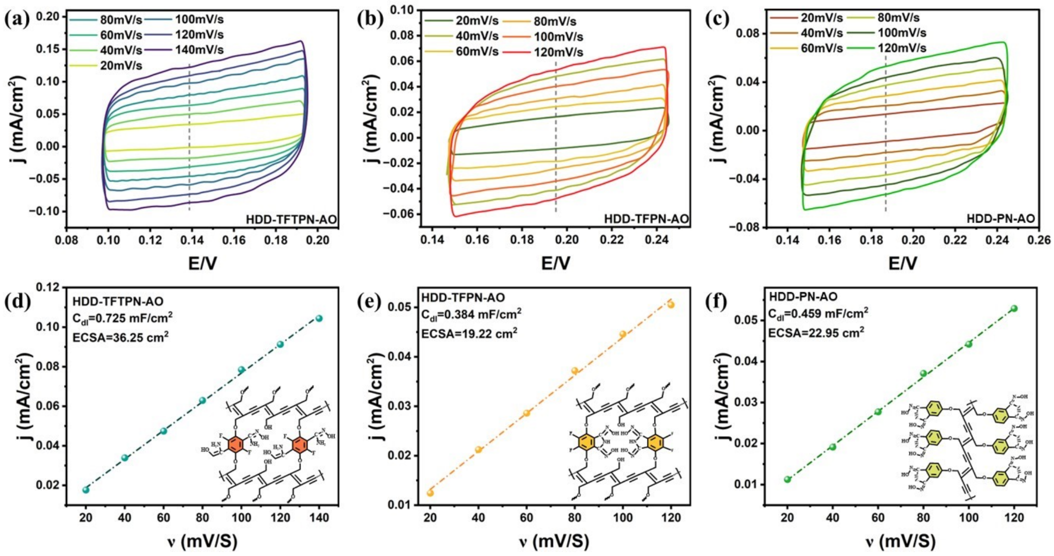

Figure S25. The linear cyclic voltammetry of **HDD-TFTPN-AO (a), HDD-TFPN-AO (b)** and **HDD-PN-AO (c).** The Electric double layer capacitance value (C_{dl}) and electrochemical Active Surface Area (ECSA) of **HDD-TFTPN-AO (d), HDD-TFPN-AO (e)** and **HDD-PN-AO (f).**

The HDD-TFPN-AO and HDD-PN-AO possess a similar ECSA, which is related to their similar functional groups (glutaroimide-dioxime). The HDD-TFTPN-AO is approximately twice that of other TP-COPs, which demonstrate the difference between amidoxime with glutaroimide–dioxime group.

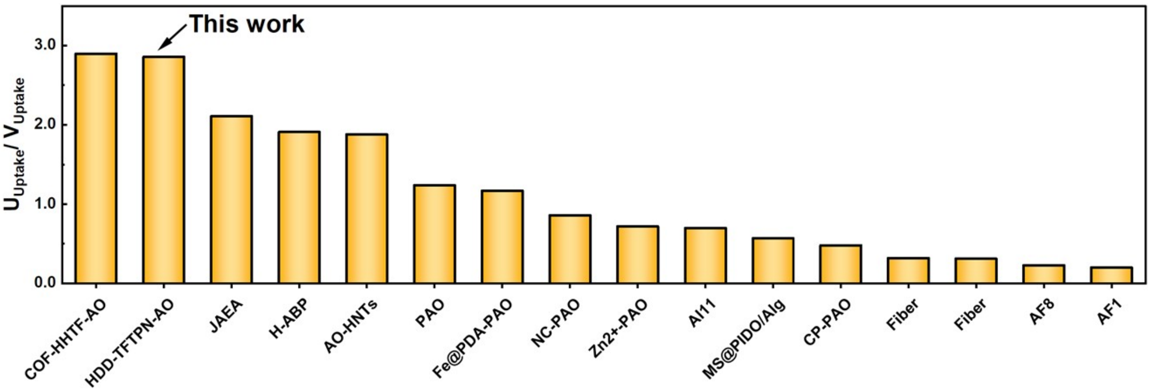

Figure S26. Comparison of U/V mass ratio with the reported adsorbent.

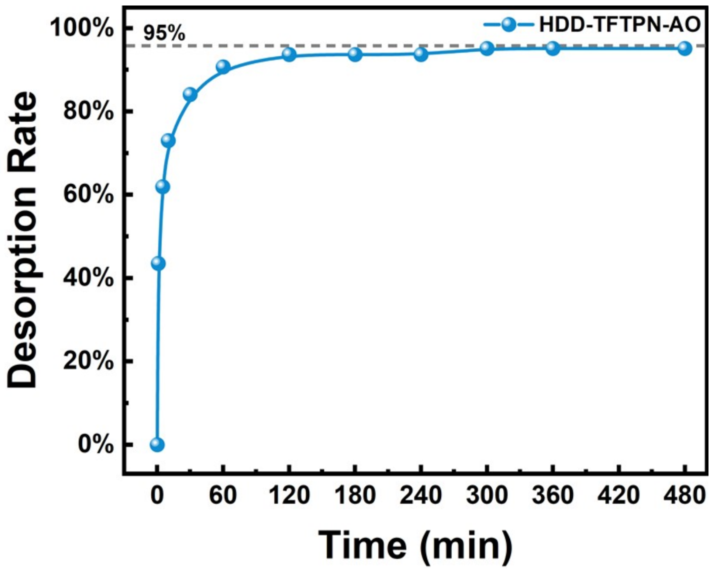

Figure S27. The desorption process of HDD-TFTPN-AO

As illustrated in Figure S25, the uranium desorption was completed within 120 min, with an initial desorption rate of 43% in the first minute, 73% at 10 minutes, and 93% at 60 minutes. According to the results of ICP-MS analysis, only 5% of uranium was remain in the adsorbent, which has a negligible impact on the adsorption performance of the material in the next cycle.

5. Tables

Table S1. Isotherm parameters for uranium extraction of three COPs.

Isotherm models	Parameters	Sample		
		HDD-TFTPN-AO	**HDD-TFPN-AO**	**HDD-PN-AO**
Langmuir	q_{max}(mg·g^{-1})	570.16	530.04	282.95
	K_L(L·mg^{-1})	0.47	0.16	0.32
	R^2	0.99	0.97	0.99
Freundlich	$1/n$	0.26	0.26	0.29
	K_f(L·mg·g^{-1}·mg$^{-1/n}$)	187.45	164.14	86.44
	R^2	0.26	0.96	0.95

Table S2. Kinetics parameters for uranium extraction of three COPs.

Sample	**Pseudo-first-order**		**Pseudo-second-order**	
HDD-TFPTN-AO	$\boldsymbol{k_1}$ **(min^{-1})**	0.363	$\boldsymbol{k_2}$ **(g·(mg·min)$^{-1}$)**	1.86*10^{-3}
	$\boldsymbol{q_e}$ **(mg·g^{-1})**	556.46	$\boldsymbol{q_e}$ **(mg·g^{-1})**	558.66
	$\boldsymbol{R^2}$	0.838	$\boldsymbol{R^2}$	0.999
HDD-TFPN-AO	$\boldsymbol{k_1}$ **(min^{-1})**	3.271	$\boldsymbol{k_2}$ **(g·(mg·min)$^{-1}$)**	1.53*10^{-2}
	$\boldsymbol{q_e}$ **(mg·g^{-1})**	458.515	$\boldsymbol{q_e}$ **(mg·g^{-1})**	460.83
	$\boldsymbol{R^2}$	0.827	$\boldsymbol{R^2}$	0.998
HDD-PN-AO	$\boldsymbol{k_1}$ **(min^{-1})**	1.377	$\boldsymbol{k_2}$ **(g·(mg·min)$^{-1}$)**	6.16*10^{-4}
	$\boldsymbol{q_e}$ **(mg·g^{-1})**	246.88	$\boldsymbol{q_e}$ **(mg·g^{-1})**	256.41
	$\boldsymbol{R^2}$	0.894	$\boldsymbol{R^2}$	0.995

Table S3. Uranium adsorption capacity comparison of **HDD-TFTPN-AO** and reported adsorbents.

Sample	**pH**	**q_{max}(mg·g^{-1})**
CMPAO[7]	6.0	251.9
COF-HHTF-AO[8]	6.0	550.1
GDT[9]	6.0	490.4
HCP-AO[10]	6.0	370.9
BHMS[11]	5.0	413.7
PMTL microspheres[12]	5.0	346.65
NDA-TN-AO[13]	5.0	589.1
BDA-TN-AO[13]	5.0	526.5
ACFs-AO[14]	5.0	191.6
HDD-TFTPN-AO (this work)	**5.0**	**570.2**
HDD-TFPN-AO (this work)	**5.0**	**530.0**
HDD-PN-AO (this work)	**5.0**	**282.9**

Table S4. Uranium uptake kinetics comparison of three TP-COPs and reported adsorbents.

Sample	Adsorption speed
TpDAB[15]	90% equilibrium achieved within 3 h.
NH_3-GO[16]	reach equilibrium at about 3 h.
MWCNTs[17]	reach equilibrium at about 60 min.
MOF-76[18]	reach equilibrium at about 5 h.
LDH/GO[19]	reach equilibrium at about 6 h.
CTPP[20]	reach equilibrium at about 72 h.
MIL-101(Cr)-Ship[21]	95% equilibrium achieved within 375 min.
AO-PCDP[22]	85.4% equilibrium achieved within 10 min.
CNFs[23]	99% equilibrium achieved within 3 h.
$[NH_4]+[COF-SO_3-]$[24]	81% equilibrium achieved within 1 h.
HDD-TFTPN-AO (this work)	90% equilibrium achieved within 20 min.
HDD-TFPN-AO (this work)	90% equilibrium achieved within 20 min.
HDD-PN-AO (this work)	90% equilibrium achieved within 10 min.

Table S5. Uranium uptake capacity from natural seawater comparison of **HDD-TFTPN-AO** and reported adsorbents.

Sample	**Time (days)**	**Uranium uptake (mg·g^{-1})**
Anti-UiO-66[25]	30	4.62
AI11[26]	56	3.35
Fiber 11[27]	56	2.20
Fiber 14[27]	56	2.60
JAEA[27]	56	1.10
AF8[28]	56	4.48
PVC-co-CPVC fibers[29]	42	5.22
JAEA PE-g-PAO[29]	42	1.71
NDA-TN-AO[13]	27	6.07
COF-HHTF-AO[8]	25	5.12
PAO Semi-IPN[30]	28	4.87
p(2DVB-VBC)-2PAN[31]	27	1.99
Fe-Nx-C-R[32]	1	1.2
Amidoxime-based UHMWPE[33]	42	2.3
CP-1:12[34]	28	0.55
POP-AO[35]	56	1.32
POP-pNH2-AO[35]	56	2.27
SUIT[36]	3	0.058
SPUIT[36]	3	0.060
AF1[26]	56	3.2
HDD-TFTPN-AO (this work)	**25**	**6.39**

Table S6. The price of several raw materials for the synthesis of three TP-COPs.

Reagent	**Cost ($\$\cdot kg^{-1}$)** [1]
K_2CO_3	0.50
$NH_2OH\cdot HCl$	1.67
Tetrafluoroterephthalonitrile	2.82
Tetrafluorophthalonitrile	1.92
4-Nitrophthalonitrile	0.40
Hexa-2,4-diyne-1,6-diol	13.21

Prices obtained from wholesale suppliers (metric ton scale).

Table S7. Synthesis cost of three TP-COPs.

Reagent	**Cost ($\$\cdot kg^{-1}$)** [1]
HDD-TFTPN-AO	6.14
HDD-TFPN-AO	5.54
HDD-PN-AO	4.52

Table S8. Selectivity of **HDD-TFTPN-AO** and reported adsorbents.

Sample	$\mathbf{U_{uptake} / V_{uptake}}$
AI11[28]	0.7
Fiber 11[29]	0.32
Fiber 14[29]	0.313
JAEA[29]	2.11
AF8[13]	0.23
COF-HHTF-AO[8]	2.90
PAO Semi-IPN[30]	1.24
AF1[26]	0.20
H-ABP fiber[37]	1.91
AO-HNTs[38]	1.88
Fe@PDA-PAO[39]	1.17
NC-PAO[40]	0.86
Zn2+-PAO[41]	0.72
MS@PIDO/Alg[42]	0.57
CP-PAO hydrogel[43]	0.48
HDD-TFTPN-AO (this work)	**2.86**

Reference

1. A. D. Meredith, T. W. Knight and R. Noe, *Separation Science and Technology*, 2014, **50**, 920-925.
2. H. Füredi-Milhofer, Z. Despotović, Z. Devide and M. Wrischer, *Journal of Inorganic and Nuclear Chemistry*, 1972, **34**, 1961-1969.
3. A. Favre-Réguillon, G. Lebuzit, J. Foos, A. Guy, A. Sorin, M. Lemaire and M. Draye, *Separation science and technology*, 2005, **40**, 623-631.
4. K. Joe, E.-H. Lee, K.-W. Kim and K. Song, *Analytical Science and Technology*, 2008, **21**, 326-331.
5. Z. Wang, R. Ma, Q. Meng, Y. Yang, X. Ma, X. Ruan, Y. Yuan and G. Zhu, *Journal of the American Chemical Society*, 2021, **143**, 14523-14529.
6. J. Liu, C. Zhao, Z. Zhang, J. Liao, Y. Liu, X. Cao, J. Yang, Y. Yang and N. Liu, *Chemical Engineering Journal*, 2016, **288**, 505-515.
7. M. Xu, T. Wang, P. Gao, L. Zhao, L. Zhou and D. Hua, *Journal of Materials Chemistry A*, 2019, **7**, 11214-11222.
8. G. Cheng, A. Zhang, Z. Zhao, Z. Chai, B. Hu, B. Han, Y. Ai and X. Wang, *Science Bulletin*, 2021, **66**, 1994-2001.
9. N. Li, J. Wu, R. Su, N. Zhang, J. Zhao and Z. Wang, *Desalination*, 2023, **545**, 116153.
10. G. Zhang, Y. Wang, X. Zhang, L. Liu, F. Ma, C. Zhang and H. Dong, *Colloids and Surfaces A: Physicochemical and Engineering Aspects*, 2022, **641**, 128508.
11. W.-R. Cui, C.-R. Zhang, R.-P. Liang, J. Liu and J.-D. Qiu, *ACS Applied Materials & Interfaces*, 2021, **13**, 31561-31568.
12. H. Gong, X. Lin, Y. Xie, L. Liu, J. Zhou, H. Liao, R. Shang and X. Luo, *Journal of Hazardous Materials*, 2021, **404**, 124151.
13. W. R. Cui, F. F. Li, R. H. Xu, C. R. Zhang, X. R. Chen, R. H. Yan, R. P. Liang and J. D. Qiu, *Angewandte Chemie*, 2020, **132**, 17837-17843.
14. X. Lu, D. Zhang, A. Tesfay Reda, C. Liu, Z. Yang, S. Guo, S. Xiao and Y. Ouyang, *Industrial & Engineering Chemistry Research*, 2017, **56**, 11936-11947.
15. R.-H. Yan, W.-R. Cui, C.-R. Zhang, X.-J. Li, J. Huang, W. Jiang, R.-P. Liang and J.-D. Qiu, *Chemical Engineering Journal*, 2021, **420**, 129658.
16. S. Verma and R. K. Dutta, *RSC advances*, 2015, **5**, 77192-77203.
17. I. I. Fasfous and J. N. Dawoud, *Applied Surface Science*, 2012, **259**, 433-440.
18. W. Yang, Z.-Q. Bai, W.-Q. Shi, L.-Y. Yuan, T. Tian, Z.-F. Chai, H. Wang and Z.-M. Sun, *Chemical communications*, 2013, **49**, 10415-10417.
19. W. Linghu, H. Yang, Y. Sun, G. Sheng and Y. Huang, *ACS Sustainable Chemistry & Engineering*, 2017, **5**, 5608-5616.
20. M. Sureshkumar, D. Das, M. Mallia and P. Gupta, *Journal of hazardous materials*, 2010, **184**, 65-72.
21. J. De Decker, K. Folens, J. De Clercq, M. Meledina, G. Van Tendeloo, G. Du Laing and P. Van Der Voort, *Journal of hazardous materials*, 2017, **335**, 1-9.
22. Y. Sun, R. Leng, X. Ma, J. Zhang, B. Han, G. Zhao, Y. Ai, B. Hu, Z. Ji and X. Wang, *Chemical Engineering Journal*, 2023, **459**, 141687.
23. B. Hu, Q. Hu, D. Xu and C. Chen, *Separation and Purification Technology*, 2017, **175**, 140-146.
24. X. H. Xiong, Z. W. Yu, L. L. Gong, Y. Tao, Z. Gao, L. Wang, W. H. Yin, L. X. Yang and F. Luo,

Advanced Science, 2019, **6**, 1900547.

25. Q. Yu, Y. Yuan, J. Wen, X. Zhao, S. Zhao, D. Wang, C. Li, X. Wang and N. Wang, *Advanced Science*, 2019, **6**, 1900002.
26. S. Das, Y. Oyola, R. T. Mayes, C. J. Janke, L.-J. Kuo, G. Gill, J. R. Wood and S. Dai, *Industrial & Engineering Chemistry Research*, 2016, **55**, 4110-4117.
27. Y. Oyola, C. J. Janke and S. Dai, *Industrial & Engineering Chemistry Research*, 2016, **55**, 4149-4160.
28. S. Das, S. Brown, R. T. Mayes, C. J. Janke, C. Tsouris, L.-J. Kuo, G. Gill and S. Dai, *Chemical Engineering Journal*, 2016, **298**, 125-135.
29. S. Brown, Y. Yue, L.-J. Kuo, N. Mehio, M. Li, G. Gill, C. Tsouris, R. T. Mayes, T. Saito and S. Dai, *Industrial & Engineering Chemistry Research*, 2016, **55**, 4139-4148.
30. C. Ma, J. Gao, D. Wang, Y. Yuan, J. Wen, B. Yan, S. Zhao, X. Zhao, Y. Sun and X. Wang, *Advanced Science*, 2019, **6**, 1900085.
31. Y. Yue, R. T. Mayes, J. Kim, P. F. Fulvio, X. G. Sun, C. Tsouris, J. Chen, S. Brown and S. Dai, *Angewandte Chemie*, 2013, **125**, 13700-13704.
32. H. Yang, X. Liu, M. Hao, Y. Xie, X. Wang, H. Tian, G. I. Waterhouse, P. E. Kruger, S. G. Telfer and S. Ma, *Advanced Materials*, 2021, **33**, 2106621.
33. Z. Xing, J. Hu, M. Wang, W. Zhang, S. Li, Q. Gao and G. Wu, *Science China Chemistry*, 2013, **56**, 1504-1509.
34. Y. Yue, X. Sun, R. T. Mayes, J. Kim, P. F. Fulvio, Z. Qiao, S. Brown, C. Tsouris, Y. Oyola and S. Dai, *Science China Chemistry*, 2013, **56**, 1510-1515.
35. Q. Sun, B. Aguila, J. Perman, A. S. Ivanov, V. S. Bryantsev, L. D. Earl, C. W. Abney, L. Wojtas and S. Ma, *Nature communications*, 2018, **9**, 1644.
36. L. Tang, S. Ren, T. Zhang, X. Wei, M. Li, X. Yin and S. Wei, *Chemical Engineering Journal*, 2021, **425**, 130589.
37. X. Xu, H. Zhang, J. Ao, L. Xu, X. Liu, X. Guo, J. Li, L. Zhang, Q. Li and X. Zhao, *Energy & Environmental Science*, 2019, **12**, 1979-1988.
38. S. Zhao, Y. Yuan, Q. Yu, B. Niu, J. Liao, Z. Guo and N. Wang, *Angewandte Chemie*, 2019, **131**, 15121-15127.
39. T. Liu, Z. Xie, M. Chen, S. Tang, Y. Liu, J. Wang, R. Zhang, H. Wang, X. Guo and A. Gu, *Chemical Engineering Journal*, 2022, **430**, 133182.
40. R. Liu, S. Wen, Y. Sun, B. Yan, J. Wang, L. Chen, S. Peng, C. Ma, X. Cao and C. Ma, *Chemical Engineering Journal*, 2021, **422**, 130060.
41. B. Yan, C. Ma, J. Gao, Y. Yuan and N. Wang, *Advanced Materials*, 2020, **32**, 1906615.
42. D. Wang, J. Song, S. Lin, J. Wen, C. Ma, Y. Yuan, M. Lei, X. Wang, N. Wang and H. Wu, *Advanced Functional Materials*, 2019, **29**, 1901009.
43. J. Gao, Y. Yuan, Q. Yu, B. Yan, Y. Qian, J. Wen, C. Ma, S. Jiang, X. Wang and N. Wang, *Chemical Communications*, 2020, **56**, 3935-3938.